IOP Conf. Series: Materials Science and Engineering **163** (2017) 012006 doi:10.1088/1757-899X/163/1/012006

FEM analysis of an single stator dual PM rotors axial synchronous machine

L N Tutelea[1], S I Deaconu[2] and G N Popa[2]

[1]Politehnica University of Timisoara, Electrical Engineering Department, Vasile Parvan str., no. 1-2, 300223 Timisoara, Romania
[2]Politehnica University of Timisoara, Department of Electrical Engineering and Industrial Informatics, 5 Revolution Street, Hunedoara, 331128, Romania

E-mail: sorin.deaconu@fih.upt.ro

Abstract. The actual e - continuously variable transmission (e-CVT) solution for the parallel Hybrid Electric Vehicle (HEV) requires two electric machines, two inverters, and a planetary gear. A distinct electric generator and a propulsion electric motor, both with full power converters, are typical for a series HEV.
In an effort to simplify the planetary-geared e-CVT for the parallel HEV or the series HEV we hereby propose to replace the basically two electric machines and their two power converters by a single, axial-air-gap, electric machine central stator, fed from a single PWM converter with dual frequency voltage output and two independent PM rotors. The proposed topologies, the magneto-motive force analysis and quasi 3D-FEM analysis are the core of the paper.

1. Introduction

The (AFPM) machine (the permanent magnet machine with an axial flux), which is known also called the disc-type machine, as well, is an attractive substitute because of its shape resembling a pancake, solid(tight) compact constructions and high power density. AFPM motors are particularly especially advisable (applicable) in case of the electrical vehicles, ventilators, valve supervision, machine tools, robots and industrial [1], [2].

Axial flux machinery has been a part of the specialized literature since the early 70's, followed by the motors based on axial flux induction a couple of years later [3-6]. At the moment, direct drive appliances which are based upon actuators or low-speed generators with increased torques have drawn attention once again to the axial flux machines, particularly to the more capable ones when it comes to increased torque density and to the efficient ones (such as the PM variety) [3], [7-11].

However, every time a couple of design goals are met, the AFPM synchronous machines are a good option to consider. More exactly, it's a common fact that the number pole pairs have to be comfortably high [3], [12].

It is also a common occurrence that the fractional slot windings can be manufactured in robust outlines. This is the case when the windings extensions are not overlapped and the stator teeth are surrounded by single coil windings. Fractional slot robust windings provide consistent assets to the end user. Actually, their usage grants a physical phase separation between the phases and of the magnetic circuits of the phases, resulting in a reduced exposure to issues between the phases and also decreasing the reciprocal inductance during the phases [3], [13].

The common material used for the back cores of the AFPM synchronous machines is the laminated steel. However, Soft Magnetic Composites (SMC) are heavily considered because of their match with increased frequencies and their reduced weight [3].

The coveted increased achievements may be obtained by the usage of PM machines and different supervision ways, one of which the direct torque control (DTC) or other increased performance vector management methods stand out [14].

This study nominates a brand new dual PM rotor, SM run with basically a single stator (with a Gramme-ring or dual winding, placed on either extremities of the stator) and dual rotor equipped with distinct leg calculations and increased winding elements, in order to decrease the size, the mass and the expenditure for both series and parallel planetary-gear HEVs. The paper is organized as follows: Section 2: constructive elements, Section 3: concentrated winding axial PM synchronous machine, Section 4: analytical quasi – 3D modeling, Section 5: FEM analysis, Section 6: conclusions.

2. Constructive elements

In the first figure the scheme of the machine seen from the front and from the side is presented.

The single stator dual PM rotors axial synchronous machine with the centred stator cluster (1) with two three-phase windings (2) found in free sockets fixed rigid in the casing (3), coming with two extremity covers (4), (5) in which the two ball bearing backings(6), (7), radial and axial, are put. The ball bearings create the possibility that the two shafts (8), (9) will pivot each on its own, each shaft having a solid steel platter (on which the permanent magnet extremities are arranged in a circular and symmetric fashion) placed towards the stator. The other end of the shaft is is added into a half-coupling linked to the thermal engine (10), respectively to the gears placed against the drive wheels (11).

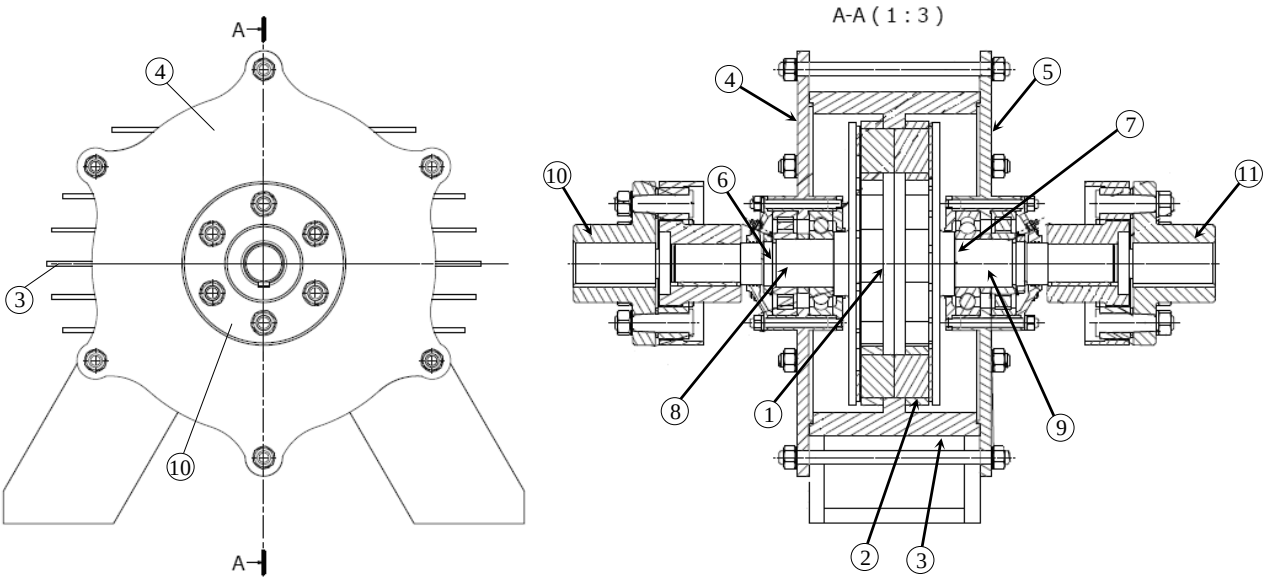

Figure 1. Front view and longitudinal section through the dual PM rotors machine

For the stator magnetic core soft magnetic composite (SMC) is suggested, but a rolle-laminated magnetic core works just as fine. The same explanation is true in case of the rotors magnetic core.

A surface-mounted PM design has been taken into account for the rotors, 14 poles for rotor 1 and 10 poles for rotor 2 (Figure 2).

The material of the permanent magnets is the Neodymium Iron Boron (Nd-Fe-B) type MPN 40SH, with flux density remanence B_r = 1,13T and cohercitive field intensity $H_c = 860 \cdot 10^3 A/m$.

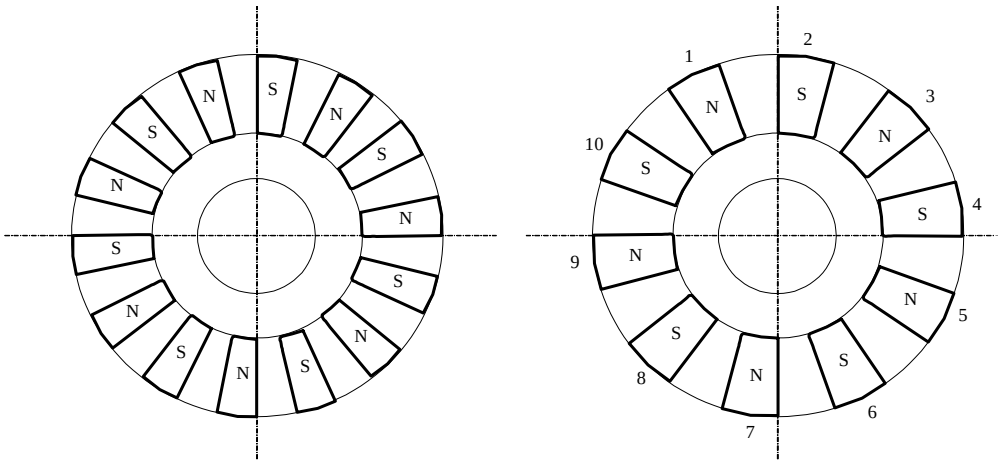

a) b)

Figure 2. Rotor 1 with 14 PM poles (a) and rotor 2 with 10 PM poles (b)

3. Concentrated winding axial PM synchronous machine

3.1. Armature Windings Design

An AFPM machine can compete with the traditional radial-flux machines in terms of torque and power density if the number of pole-pairs is sufficiently high and the ratio axial length/outer diameter is low [1], [3], [12].

The various combinations of slots and poles which allow the realization of balanced winding can be determined by the relation:

$$\frac{N_{st}}{\left[GCD\left(N_{st},2p\right)\right]}=3k \ , \tag{1}$$

where N_{st} is the number of slots, p the number of pole pairs and k an integer number (GCD: Greatest Common Divisor). As is well known, the number of slots per pole and per phase of an electrical machine is equal to:

$$q=\frac{N_{st}}{2pm} \ , \tag{2}$$

where m is number of phases.

Fixing N_{st}, if the machine has a high number of pole pairs, q decreases.

In concentrated non-overlap windings, there is only one coil in a coil group or coil phase belt (z = 1). The distribution factor for the fundamental space harmonic is calculated by [1]:

$$k_{d1}=\frac{sin\left(\frac{\pi}{2m}\right)}{z\cdot sin\left(\frac{\pi}{2mz}\right)} \ , \tag{3}$$

and the pitch factor for the fundamental space harmonic is [1]:

$$k_{p1}=sin\left(\frac{\pi}{2}\cdot\frac{y}{\tau}\right) \ , \tag{4}$$

where y is the pitch of one coil and τ the pole pitch. The fundamental winding factor:

$$k_{w1}=k_{d1}\cdot k_{p1} \ , \tag{5}$$

For our case k_{w1} = 0.966 for both windings. (N_{st}=12, p_1 = 7, p_2 = 5).

Figure 3 and Figure 4 shows the AFPM windings layout.

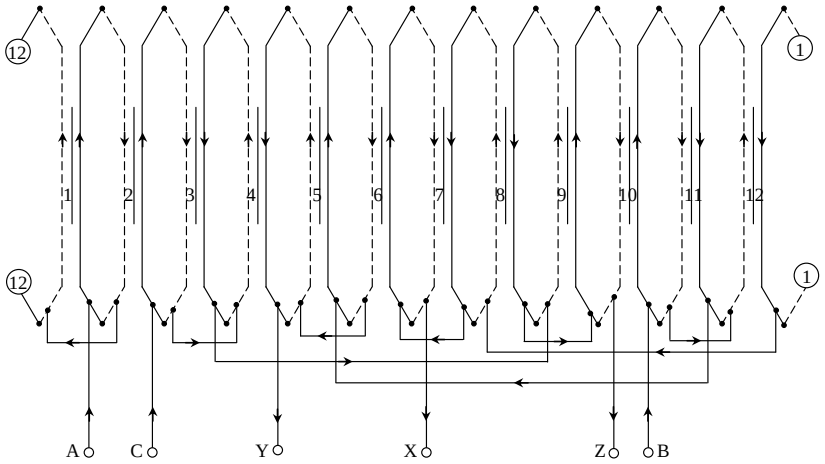

Figure 3. AFPM winding arrangement (N_{st}=12, p=7, m=3)

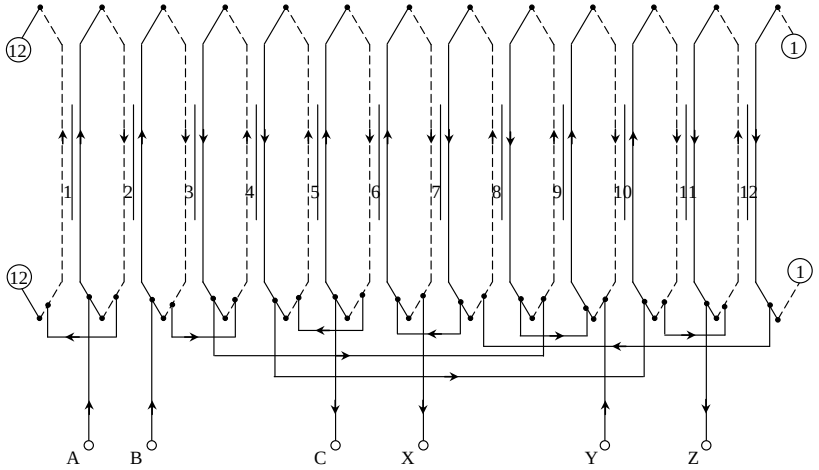

Figure 4. AFPM winding arrangement (N_{st}=12, p=5, m=3)

3.1. MMF Analysis

The parameter τ is the average pole pitch.

$$\tau = \frac{\pi D}{2p} \ , \tag{6}$$

where D is the average diameter

$$D = \frac{D_{out} + D_{in}}{2} \ , \tag{7}$$

with D_{out} the outer and D_{in} the inner diameter of machine.

The MMFs F_{ad} and F_{aq} in the d-axis and q-axis are [1]:

$$F_{ad} = \frac{m_1\sqrt{2}}{\pi} \cdot \frac{N_1 \cdot k_{w1}}{p} \cdot I_{ad} \ , \tag{8}$$

$$F_{aq} = \frac{m_1\sqrt{2}}{\pi} \cdot \frac{N_1 \cdot k_{w1}}{p} \cdot I_{aq} \ , \tag{9}$$

where I_{ad} and I_{aq} are the d and q axis stator (armature) currents respectively.

Let us consider the case where the concentrated winding PM machine is fed by sinusoidal currents, with a maximum current I in phase "A" (i_A=I and i_B=i_C=-I/2).

In order to investigate the spatial distribution of the armature MMF, the surface mounted PMs in the rotor are supposed to be discarded. Giving the fact that each phase is made up of N coils, and accounting for the notations considered in Figure 5, the MMF F_{A1} produced by one coil $\left(\boldsymbol{A}^{+},\boldsymbol{A}^{-}\right)$ is expressed as [15]:

$$F_{A1}(\theta)=\begin{cases}(2-\beta)\cdot\dfrac{N\cdot I}{8}, & -\dfrac{\delta}{2}<\theta<\dfrac{\delta}{2}\\ -\beta\cdot\dfrac{N\cdot I}{8}, & \textit{elsewhere}\end{cases}, \tag{10}$$

where β is the coil pitch ratio, such that

$$\beta=\frac{\delta}{\tau_{st}}\ , \tag{11}$$

where τ_{st} is the armature pole pitch. Taking into account the hypothesis which considers that the magnetic circuit is not saturated, one can apply the superposition theorem in order to obtain the magneto-motive force (MMF) $F_A(\theta)$ of phase "A" as follows:

$$F_A(\theta)=F_{A1}(\theta)+F_{A2}(\theta)+F_{A3}(\theta)+F_{A4}(\theta)\ , \tag{12}$$

with

$$\begin{cases}F_{A2}(\theta)=-F_{A1}\left(\theta-\dfrac{\pi}{6}\right)\\ F_{A3}(\theta)=-F_{A1}(\theta-\pi)\\ F_{A4}(\theta)=F_{A1}\left(\theta-\dfrac{7\pi}{6}\right)\end{cases}, \tag{13}$$

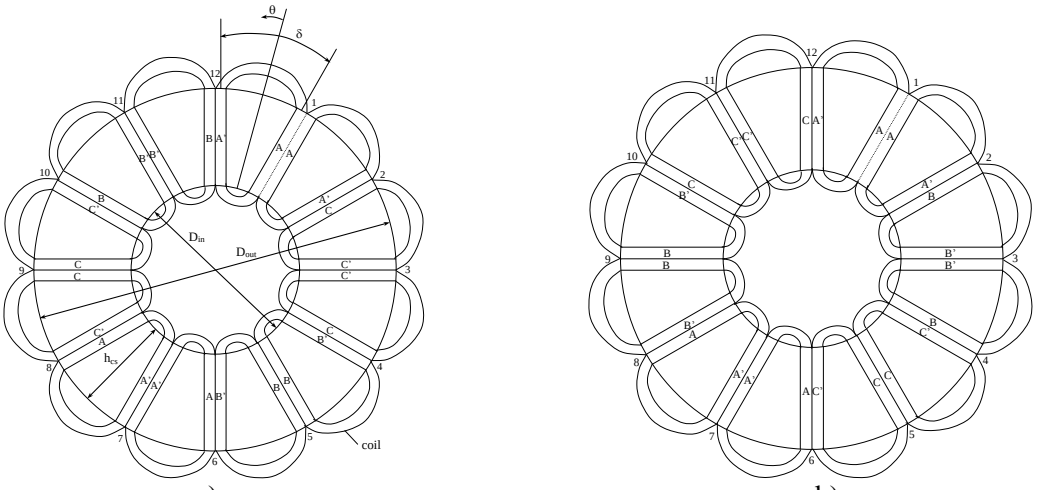

Figure 5. Two-dimensional view of the proposed three phase concentrated winding surface-mounted PM machine with N_{st}=12 slots. a) p=7 and b) p=5 pole pairs

Now let us consider the spatial distribution of the MMFs produced by phases "B" and "C", witch are deduced from the one produced by phase "A" as follows:

$$\begin{cases}F_B(\theta)=-\dfrac{1}{2}F_A\left(\theta+\dfrac{2\pi}{3}\right)\\ F_C(\theta)=-\dfrac{1}{2}F_A\left(\theta-\dfrac{2\pi}{3}\right)\end{cases}, \tag{14}$$

Then, the superposition of F_A, F_B and F_C has let to the spatial profile of the resulting armature MMFs F(θ).

4. Analytical Quasi-3D Modelling

Concerning the quasi-3D modeling the axial-flux PM machine may be considered to be composed of several axial-flux machines with differential radial length. The overall performance of an axial-flux machine is obtained by summing the performance of individual machines and by neglecting the possible flux flow in the depth direction of the machine [14]. This approach allows the consideration of different magnet shapes and variations of the teeth width in the direction of the machine radius. The method of transforming the 3D geometry of an axial-flux machine to a corresponding 2D model, to be used in quasi-3D computation, is illustrated in Figure 6.

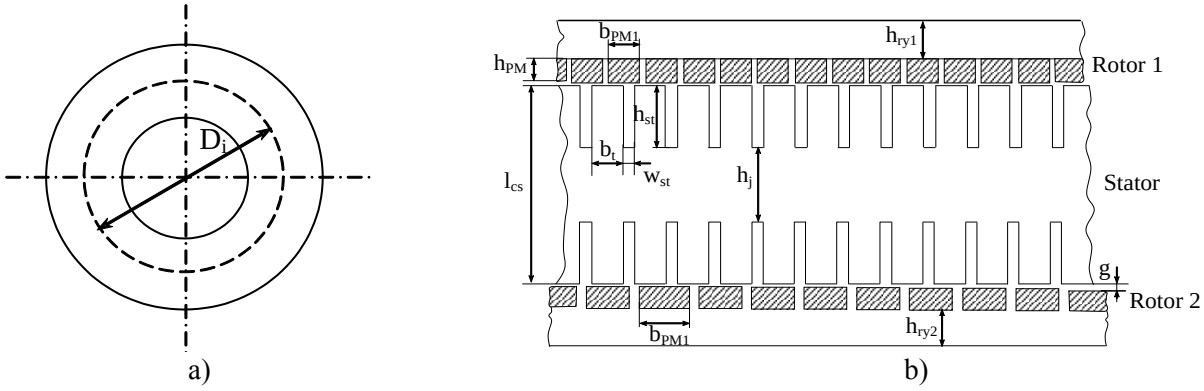

Figure 6. The selected i computation plan. a) selected i plan and b) 2D model of plan

For the quasi-3D computation, the average diameter D_i of a particular computation plan i, starting from the outer diameter of the machine is given by the equation [14]:

$$D_i = D_{out} - j \cdot \frac{h_{cs}}{N_p} \ , \tag{15}$$

where N_p is the number of computation planes used in a computation and h_{cs} is the length of the stator stack. The parameter j is defined as

$$j = 2i - 1 \ , \tag{16}$$

where index i goes from 1 to N_p. The length of the stator stack h_{cs} is defined as:

$$h_{cs} = \frac{D_{out} - D_{in}}{2} \ . \tag{17}$$

The pole pitch for each computation plane is given by the equation:

$$\tau_i = \frac{\pi D_i}{2p} \ . \tag{18}$$

Based on the set of equations (15)-(18) it is possible to divide the machine into a certain amount of computation planes. The number of computation plans needed for computation depends on the purpose (precision) of the computation.

5. Quasi – 3D FEM analysis

When applied to electrical machines, the described problem is usually reduced to cover only one pole or one pole pair with the help of boundary and symmetry conditions in order to reduce the computation time. In addition, it is often sufficient to reduce the problem to a 2D plane and use the finite element analysis (FEA). A finite element program enabling the modelling of linear movement is recommended [14], [16].

The main parameters of the model are given in Table 1.

The windings are in star connections and thus the current shares among phases are $I_A = I$, $I_B = I_C = -\frac{I}{2}$.

The computation results are calculated with the Simpson formula:

$$C = \left(C_{out} + 4C_{average} + C_{in}\right) \cdot \frac{1}{6}, \tag{19}$$

where C are result from computation and C_{out}, $C_{average}$ and C_{in} are the results from computation plane at D_{out}, D and D_{in}.

Table 1. Parameters and machine dimensions

Frequency (f)	50 Hz
Number of poles rotor 1	14
Number of poles rotor 2	10
Current density (J_s)	5.83 A/mm^2
Air-gap length (g)	2 mm
Outer diameter (D_{out})	260 mm
Inner diameter (D_{in})	156 mm
Pole-arc-ratio rotor 1 (α_{i1})	1
Pole-arc-ratio rotor 2 (α_{i2})	0.6944
Number of stator slots (N_{st})	12
Slot depth (h_{st})	21 mm
Axial length of stator core (h_{cs})	72 mm
Axial length of rotor 1 core (h_{ry1})	15 mm
Axial length of rotor 2 core (h_{ry2})	17.5 mm
Magnet axial length (h_{PM})	5 mm
PM rotor 1 width (b_{pm1})	38.6 mm
PM rotor 2 width (b_{pm2})	54.1 mm
Permanent magnet material	Ne Fe B

Figure 7 shows the finite element mesh for initial position. A background object that fills all free space between material objects is added. When the interaction forces are computed using the Maxwell tensor, it is better to design the integration path through finite elements that have all nodes in a linear medium without currents, in order to reduce the integration error. This condition could be achieved if the mesh has at least four layers in the air-gap. In order to enforce four mesh layers in the air-gap, we can define two extra regions along the air-gap with air features [16].

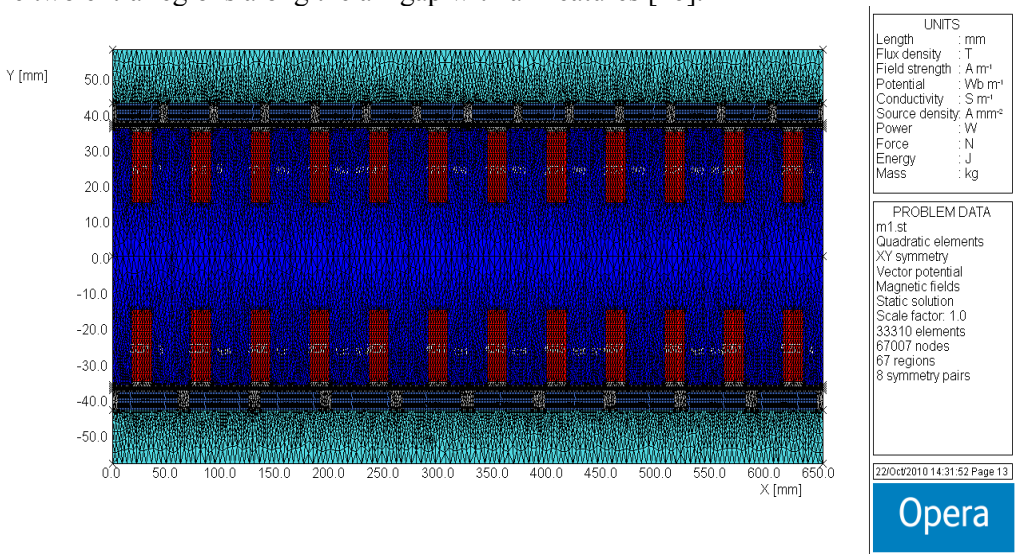

Figure 7. AFPM mesh – full problem

In our case, such a region was defined around the PM rotor 1 and PM rotor 2, placed in such a manner that it does not reach this region when it is moved. Figure 8 presents mesh details. The mesh has 67 regions, 8 symmetry pairs, 68 341 nodes and 33 958 elements.

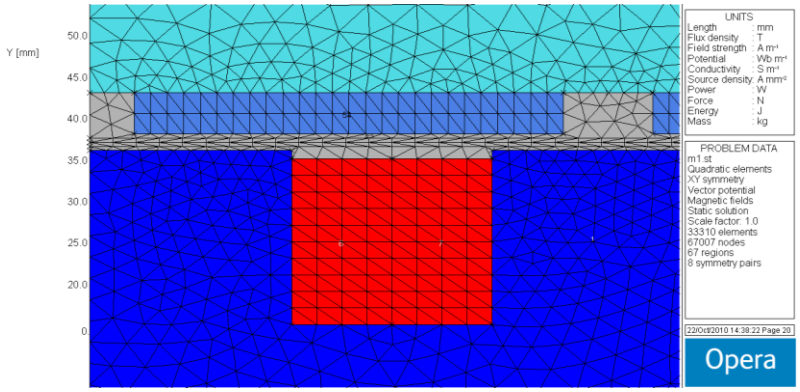

Figure 8. AFPM mesh – details

The FEM setup and magnetic field lines for initial position, are show for full load, I=720 Aturns in Figure 9.

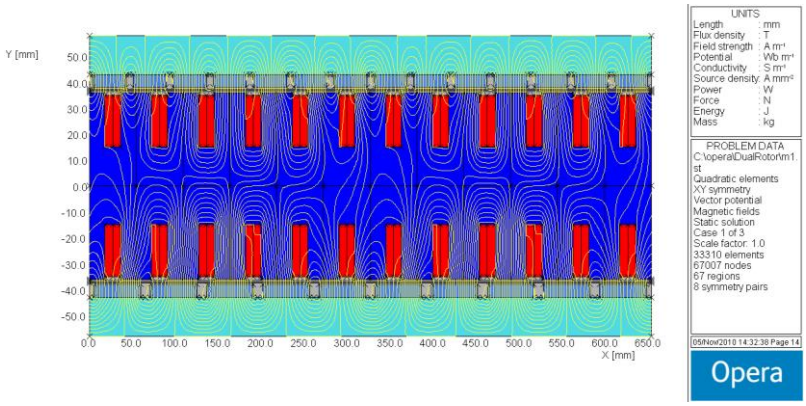

Figure 9. Magnetic field lines at I = 720 Aturns, and initial position of rotor 1

The total distribution of the flux density for initial position is presented in Figure 10 and the air-gaps flux density for rotor 1 and rotor 2 are presented in Figure 11 and Figure 12.

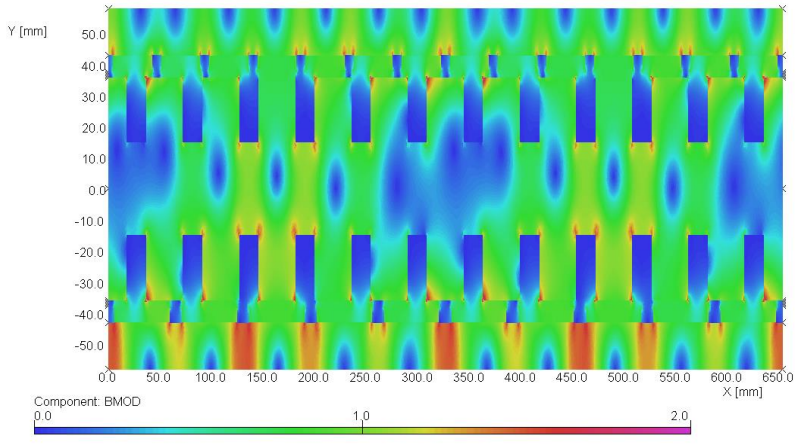

Figure 10. The total distribution of the flux density at full load (I=720 Aturns), and initial position of rotor 1

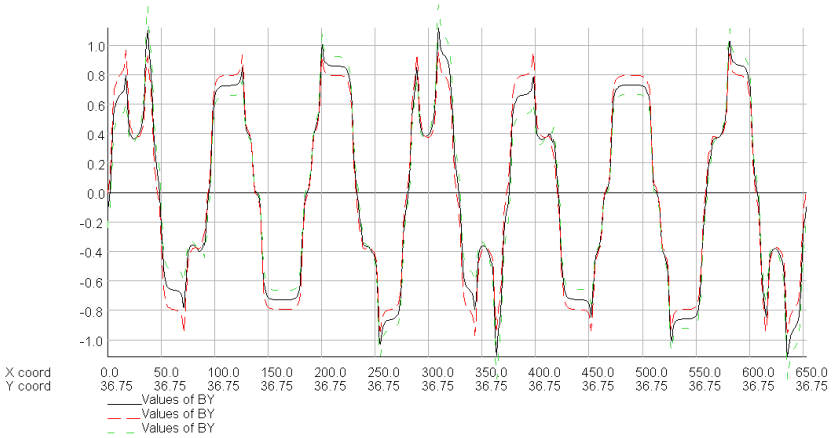

Figure 11. The air-gap 1 flux density for I = 0 (red), I=720 Aturns (black) and I = 1440 A (green)

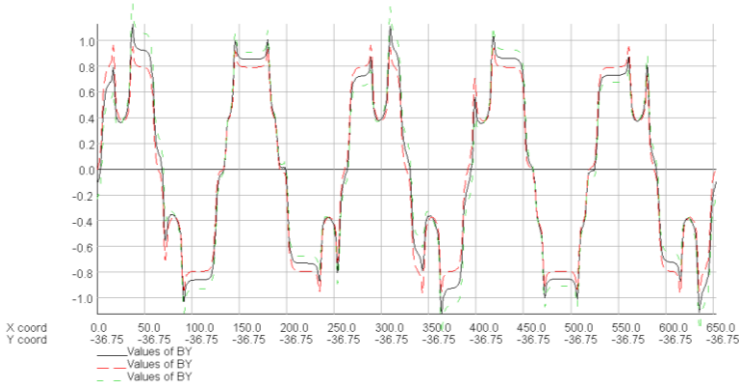

Figure 12. The air-gap 2 flux density for I = 0 (red), I=720 Aturns (black) and I = 1440 Aturns (green)

In Figure 13 is presented the magnetic induction on a pair of poles in idle run for the airgap 1, respectively 2, obtained by FEM-3D [2]. Comparing with the results presented in Figure 11 and Figure 12, one can notice that both the curves' shape and the induction values mostly coincide (3% and 3,5% maximum difference for p_1=7 and p_2=5 respectively).

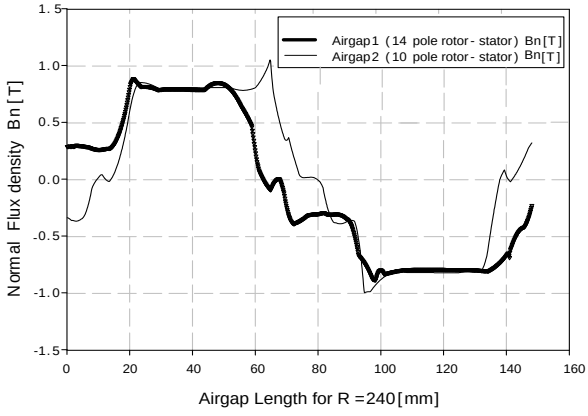

Figure 13. No load air-gap flux density variation from 3D-FEM

In quasi 3D-analysis the rotating of rotor 1 is converted in translation between rotor 1 and stator. Figure 14 presents the position of rotor 1 for maximum torque, and in Figure 15 a mesh detail for this position. The real scale between the machine's radial and axial dimensions are presented in Figure 16 (with magnetic field lines produced by the PMs – I=0).

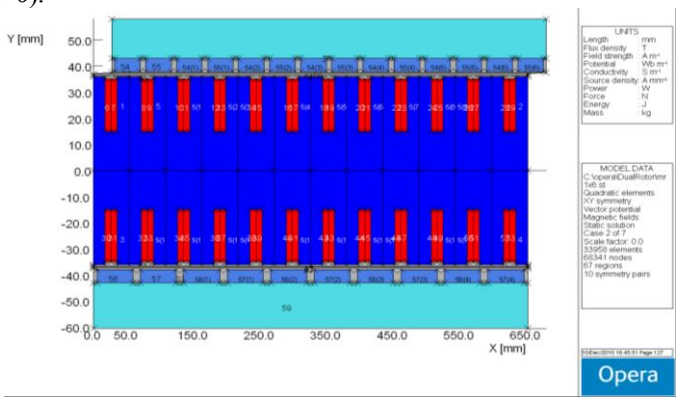

Figure 14. Computational average plan with rotor 1 in maximum torque position

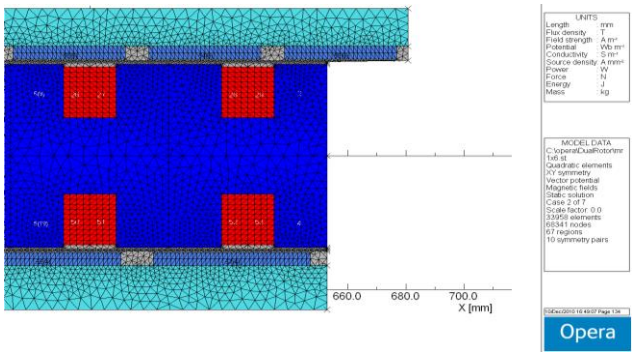

Figure 15. Mesh details at maximum torque position of rotor 1

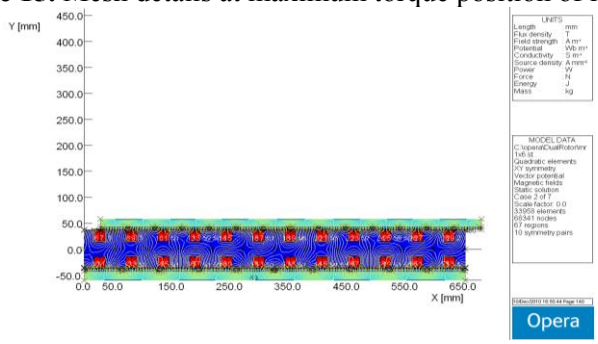

Figure 16. Real scale of the machine. Magnetic field lines with rotor 1 in maximum torque position. I=0

The computation was made with seven factor scale current and τ displacement of rotor 1 in ten intermediary positions. The results are for phase a1 flux (Figure 17), for PM flux in rotor 1 and rotor 2 (considered stationary) (Figure 18), for tangential and axial forces for rotor 1 in Figure 19 and Figure 20. The inductance variation is very low with position (Figure 21) and the torque (Figure 22) is comparable with the value computed by 3D FEM analysis (Figure 23) (3,7% maximum difference) [2]. The cogging torque is very low (I=0 Figure 22).

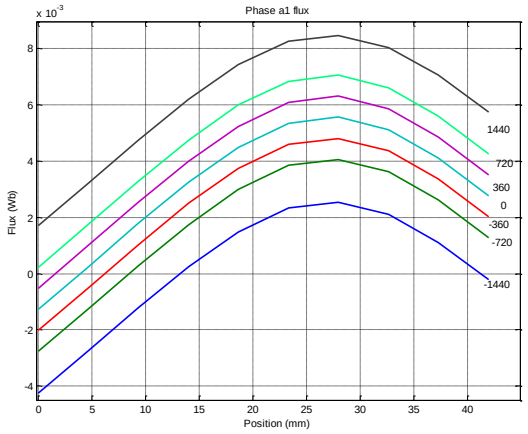

Figure 17. Phase a1 flux at seven factor scale current

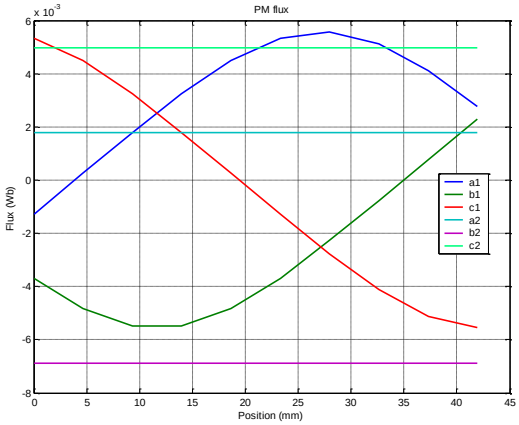

Figure 18. PM flux in rotor 1 and rotor 2

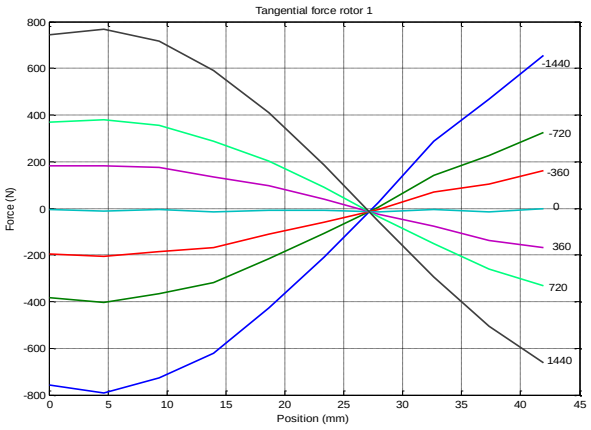

Figure 19 Tangential force rotor 1 for seven factor scale current

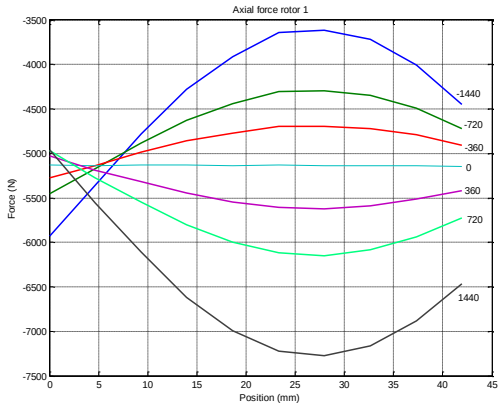

Figure 20. Axial force rotor 1 for seven factor scale current

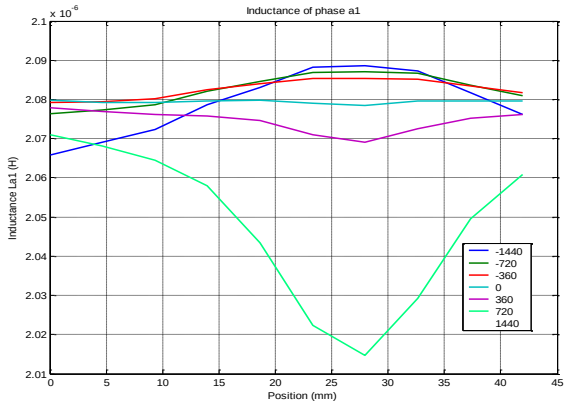

Figure 21. Inductance per phase at seven factor scale current

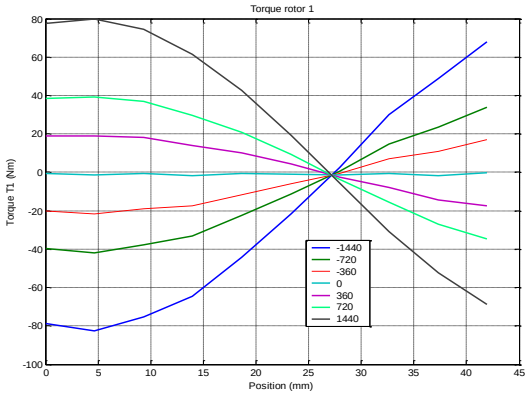

Figure 22. Torque of rotor 1 at seven factor scale current

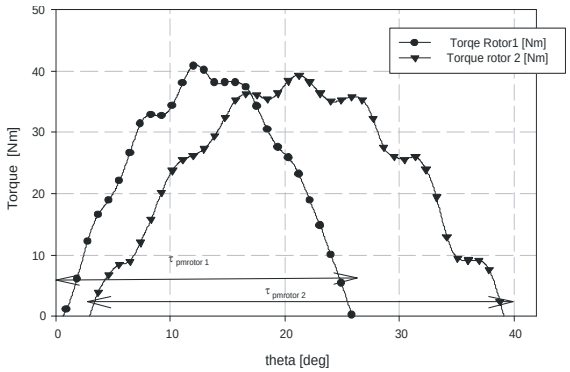

Figure 23. 3D Analysis torque for the two rotors

Comparing the results obtained by the quasi-3D method with 3D-FEM (2,1% mean square error for torque calculation), is noticed that both the torque and the magnetic induction in the air gap have closed variation forms and values. The results of the quasi-3D analysis were obtained for three calculation plans at diameters D_{in}, D and D_{out}. For a higher precision can be taken into account additional plans. The calculation time for 3D-FEM analysis is much bigger than for quasi-3D. From here, it results the advantage of using this type of analysis.

6. Conclusions

Using an analytical design method or the 2D finite element analysis (FEA) only for the average radius on the machine does not generally yield sufficiently accurate computation results. With the 3D FEA, it is possible to take into consideration the actual 3D structure of the machine, but performing the computations is too often time-consuming, especially if the objective is to achieve a preliminary design of the machine.

The basic idea of the hereby proposed design method is to firstly subdivide the axial flux machine into a sufficient amount of independent computation plans, next perform the required 2D computations on each plane, and finally compose the overall performance of the machine from the computation results obtained for each design plan.

References

[1] Gieras J F, Wang R J and Kamper M J 2008 *Axial Flux Permanent Brushless Machines*, Second Edition, Springer Science, Boston, MS USA

[2] Boldea I, Topor M, Marignetti F, Deaconu S I and Tutelea L N 2010 *A Novel Single Stator Dual PM Rotor, Synchronous Machine: topology, circuit model, controlled dynamics simulation and 3D FEM Analysis of Torque Production*, 12th International Conference on Optimization of Electrical and Electronic Equipment OPTIM 2010, Brasov, Romania, May 20-22, pp 343-351

[3] Marignetti F, Colli V D, Di Stefano R and Cavagnino A 2007 D*esign Issues of a Fractional – Slot Windings Axial Flux PM Machine with Soft Magnetic Compound Stator*, IECON 2007, Taipei, Taiwan, November 5-8, pp 187-192

[4] Campbell P 1974 Principles of a permanent magnet axial-field DC machine*, Proceedings IEE* **121**(12) 1489-1494

[5] Campbell P 1975 The magnetic circuit of an axial field DC electrical machine, *IEEE Transactions on Magnetics* **11**(5) 1541-1543

[6] Leung W 1978 *Sandwich synchronous machines and DC machines*, patent specifications, London, UK

[7] Profumo F, Zhang Z and Tenconi A 1997 Axial flux machine drives a new viable solution for electric cars, *IEEE Transaction on Industrial Electronics* **44**(1) 39-45

[8] Eastham J F, Profumo F, Tenconi A, Hill-Cottingham R J, Coles P C and Gianolio G 2002 Novel Axial flux Machine for aircraft drive: design and modeling, *IEEE Transactions on*

Magnetics **38**(5) 3003-3005
[9] Brooking P and Bumby J R 2002 A*n integrated engine-generator set with power electronic interface for hybrid electric vehicle applications*, International Conference on Power Electronics, Machines and Drives, June 4-7, pp 153-158
[10] Cavagnino A, Lazzari M, Profumo F and Tenconi A 2002 A comparison between the axial flux and the radial flux structures for PM synchronous motors, *IEEE Transactions on Industrial Applications* **38**(6) 1517-1524
[11] Sitapati K and Krishnan R 2001 Performance Comparisons of Radial and Axial Field, permanent-Magnet, Brushless Machines, *IEEE Transactions on Industrial Applications* **37**(5) 1219-1226
[12] Marignetti F and Scarano M 1999 *An Axial-flux PM Motor Wheel*, Electromotion'99, Patras, Greece, pp 1-6
[13] Cros J and Viarouge Ph 2002 Synthesis of High performance PM Motors with Concentrated Windings, *IEEE Transactions on Energy Conversion* **17**(2) 248-253
[14] Parviainen A 2005 *Design of AFPM low-speed Machines and Performance Comparison between Radial-Flux and Axial-Flux Machines*, Lappeenranta University of Technology, Finland, Doctoral Thesis
[15] Hamadou G B, Masmoudi A, Abdennadher I and Masmoudi A 2009 Design of a Single-Stator Dual-Rotor Permanent-Magnet Machine, *IEEE Transactions on Magnetics* **45**(1) 127-132
[16] Boldea I and Tutelea L N 2009 *Electric Machines. Steady State, Transients and Design with MATLAB*, CRC Press